Journal of Theoretical Biology 263 (2010) 455–470

Contents lists available at ScienceDirect

Journal of Theoretical Biology

journal homepage: www.elsevier.com/locate/yjtbi

A mechanomolecular model for the movement of chromosomes during mitosis driven by a minimal kinetochore bicyclic cascade

Blerta Shtylla, James P. Keener *

Mathematics Department, University of Utah, Salt Lake City, UT, USA

ARTICLE INFO

Article history:
Received 8 May 2009
Received in revised form
17 December 2009
Accepted 22 December 2009
Available online 4 January 2010

Keywords:
Chromosome oscillations
Diffusive coupler model
Mitotic kinases

ABSTRACT

During mitosis chromosomes use a complex network of dynamic microtubules to find the cell equator in preparation for division signals. The roles of cellular chemical signals in mechanisms driving mitotic chromosomal movements are not well understood. In this paper we propose a mathematical model of this process which incorporates a molecular scale model of kinetochore–microtubule interactions into a negative feedback loop between spindle forces and local kinetochore biochemical reactions. This system allows kinetochore biochemical reactions to control and coordinate chromosome movement thus providing a direct connection between mechanical signals and mitosis chemical species. Our feedback control model can recreate chromosome movement from prometaphase to anaphase in good agreement with experimental data.

1. Introduction

The movement of chromosomes to the cell equator is one of the most striking mitotic events. Chromosome motility is facilitated by the mitotic spindle, which consists of a complex network of microtubules (MT) that nucleate from two poles. The spindle machinery essentially lays out a system of tracks on which chromosomes move. Mechanical linkage between chromosomes and microtubules is provided by proteinaceous structures called kinetochores (Kt) (Cheeseman and Desai, 2008). Depending on its attachment to the spindle a chromosome can be in one of two states: monooriented if it is tethered to microtubules from only one pole, or bioriented if connected to microtubules from both poles.

In many vertebrate cells, monooriented and bioriented chromosomes show oscillatory movements classified as "directional instability" (Skibbens et al., 1993). Oscillatory motility is characterized by periods of motion at approximately constant speeds marked by abrupt switches between motion directed toward and away from a pole (Skibbens et al., 1993; Rieder and Salmon, 1994). We refer to chromosome motion directed toward the closest pole to which it is tethered as poleward motion and motion away from the closest pole as antipoleward (AP) motion. Toward and away from pole movements have been shown to be primarily coupled to Kt associated microtubule (kMT) growth/shortening by tubulin addition/removal at the attachment site (Mitchison and Salmon, 1992). Typically a chromosome becomes first monooriented and travels toward the pole from which the kMT nucleated. Once close to this pole, it experiences directional instability awaiting connections from the opposing pole. After biorientation, motion preserves constant velocities with a bias toward the spindle equator controlled by the duration of poleward and antipoleward trips (Skibbens et al., 1993). At the end of metaphase chromosomes align at the cell equator and undergo further oscillations.

Poleward chromosome movement results from forces arising at kinetochores. In turn, kinetochore forces could originate from Kt coupling to depolymerizing microtubules or the pulling action of minus-end directed motor proteins. Several motor proteins such as dyneins, CENP-E are found at kinetochores (Cheeseman and Desai, 2008). Even though molecular motor enzymes are likely to contribute to kinetochore tethering to kMTs, their role in generating motion is questioned on the basis that molecular motor depletion in higher eukaryotes does not entirely hinder Kt/kMT interactions (Kapoor et al., 2006), and their activity is dispensable for chromosome motility in yeast (Tanaka et al., 2007; Grishchuk and McIntosh, 2006). Therefore, it seems reasonable to expect chromosome poleward movement to depend on kinetochore coupling to kMT tip shortening rates.

Interactions between spindle MTs and chromosome arms could be sufficient for antipoleward motion provided that kinetochores are tethered to growing kMTs. Astral microtubules push chromosome arms away from the poles toward the spindle equator creating what are known as "polar ejection" forces (Rieder and Salmon, 1994; Rieder et al., 1986). The interactions between the spindle and chromosome arms at a given position depend on the density of microtubules there. For equal densities of microtubules emanating from each pole the polar ejection

* Corresponding author. Tel.: +1 801 581 6089; fax: +1 801 585 1640.
E-mail address: keener@math.utah.edu (J.P. Keener).

0022-5193/$ - see front matter © 2009 Elsevier Ltd. All rights reserved.
doi:10.1016/j.jtbi.2009.12.023

forces should balance half way, at the spindle equator. Therefore, polar ejection forces provide spatial cues which guide chromosomes to the cell equator.

Since movement seems to depend on the coordination of the forces exerted on kinetochores with kMT tip rates, a mechanism for local Kt control that incorporates force dependent kMT tip rate regulation could be sufficient to generate motion. Indeed, local motility control at kinetochores is supported by evidence that chromosomes in the same cell move autonomously with uncoordinated directional switches (Skibbens et al., 1993; Rieder and Salmon, 1994). Also, tension arising from stretching of sister kinetochores during oscillations has been implicated in controlling transitions from poleward to AP motion (Skibbens et al., 1993). More importantly, there is evidence for a kinetochore force mediated regulatory mechanism based on experiments which have identified Kt associated force sensing proteins that also affect kMT polymerization/depolymerization rates (Sandall et al., 2006; Gorbsky, 2004; Lampson et al., 2004; Bolton et al., 2002; Murata-Hori and Wang, 2002). The details of how such a biochemical-force regulatory machinery could work to control chromosome motility are not well understood.

A previous model by Gardner et al. (2005) studied how kinetochore force sensing affects chromosome motility in yeast where kinetochores only bind a single MT. This study, however, did not specify how kinetochores sustain attachment or address any explicit mechanisms that would integrate mechanical tension with velocity modulation at kinetochores. Recently Liu et al. (2008) considered a chemical reaction mechanism for chromosome motility where velocity control was purely chemical with no explicit load dependence or variation in attachment numbers at each kinetochore. While kinetochores seem to operate on flat load velocity curves with velocities insensitive to load variations, any coupler motor would have to eventually adjust its response if loads became too large. We reasoned that these effects could be important in chromosome motility and thus sought to investigate them explicitly in a chromosome motility model.

In this paper we develop a model of chromosome movement where velocity is controlled by a negative feedback mechanism between spindle forces and kinetochore localized force dependent chemical reactions. For each chromosome attachment site we build a model that describes the molecular mechanics of the Kt/MT connection. Then, we use the corresponding load–velocity relationships to predict system velocity in response to various Kt loads and kMT tip rates. The proposed feedback mechanism generates independent chromosome oscillations in the monooriented case, and predicts congression and further oscillations in the bioriented state, in good agreement with data.

2. Model

In this section we describe model assumptions and equations.

In Fig. 1 is shown a diagram of a chromosome and of all the forces included in our model that affect its motion. We suppose that chromosome movement is in the horizontal direction along a one dimensional axis starting from the left pole (at $x=0$) to the right pole (at $x=L$). Furthermore, we assume that the motion is viscous dominated (inertia can be neglected) so that

$$v\frac{dx_j}{dt}=\sum F, \tag{1}$$

where x_j is the x-coordinate position of a chromosome arm, v is the viscosity, and $\sum F$ is the sum of all applied forces. Three types of forces are included in our model. These are: (1) polar ejection forces due to spindle MTs, (2) forces from each kinetochore molecular motor bound to a MT, and (3) forces coming from physical linkage with sister chromatids.

The individual forms for these forces are specified as follows. Polar ejection forces are assumed to arise when MTs interact with chromosome arms. Since these forces are thought to be microtubule density dependent we model their effect using an inverse square distribution law of the form $f_{ap}/x^2=k_{ap}A_{cc}/x^2$ where A_{cc} is chromosome cross sectional area parallel to the equator and x is chromosome distance from the pole (Rieder et al., 1986; Joglekar and Hunt, 2002). The parameter k_{ap} is a force density term which depends on the number of astral microtubules interacting with chromosome arms.

Kinetochore motor forces are calculated from load–velocity relationships which we derive in the next section. We allow a Kt to bind several MTs, however, each binding generates a force corresponding to a single molecular motor. The key motor model result (described below) is that when attached, a motor generates a load (or force) that depends on the motor velocity and the balance of kMT tip polymerization and depolymerization rates, identified by the depolymerization rate β_j.

Finally, cohesin complexes provide physical connection between sister chromatids (Uhlmann, 2001) and are modeled by a linear center spring.

Thus, the positions of the chromatids are governed by the equations

$$v\frac{dx_L}{dt}=\frac{1}{2}\left(\frac{f_{ap}}{x_L^2}-\frac{f_{ap}}{(L-x_L)^2}\right)-\sum_i^m F_{sL,i}\left(-\frac{dx_L}{dt},\beta_L(t)\right)+k_f(x_R-x_L-L_k), \tag{2}$$

$$v\frac{dx_R}{dt}=\frac{1}{2}\left(\frac{f_{ap}}{x_R^2}-\frac{f_{ap}}{(L-x_R)^2}\right)+\sum_i^n F_{sR,i}\left(\frac{dx_R}{dt},\beta_R(t)\right)-k_f(x_R-x_L-L_k), \tag{3}$$

where x_j $(j=L,R)$ refers to the position of the chromatid facing the jth pole (Fig. 1) with n,m the total number of attached right and left kinetochore couplers, respectively. $F_{sj,i}$ corresponds to the forces coming from i th motor attached at kinetochore j, and L_k is the cohesin spring relaxed length. For simplicity we have split the anti-poleward forces on each sister chromatid in half.

The next important ingredient of the model are the Kt chemical reactions. We propose that kinetochores contain a sensor species S which is activated at a force dependent rate subsequent to a microtubule binding a kinetochore. We assume that if S grows above a threshold value, it promotes the phosphorylation of a species A into Ap; if S decays below threshold a phosphatase takes Ap into A. Possible candidates for the sensor are components of the CPC complex and A could correspond to Aurora B (AurB), a kinetochore specific kinase. The members of the CPC complex are thought to first bind and activate AurB via force dependent phosphorylation and subsequently the kinase (auto)phosphorylates to its fully active state (Bolton et al., 2002; Sandall et al., 2006; Ruchaud et al., 2007). Since the activation of AurB is not yet completely understood we retain a simplified description where events are grouped into an activation and phosphorylation reaction. Next, the species Ap catalyzes in a threshold dependent way the phosphorylation of a mitotic kinesin, Mc. A candidate for Mc is the kinesin-13 MCAK which is a substrate of AurB at centromeres and is also the most powerful microtubule depolymerase known to date (Gorbsky, 2004; Ems-McClung et al., 2007). In line with the observation that phosphorylation of MCAK by AurB blocks its activity in vitro and in vivo (Andrews et al., 2004; Wordeman et al., 2007) phosphorylated Mc (which we denote by Mcp) is inactive in our model. Fig. 2 illustrates a wiring diagram for the kinetochore chemical reactions.

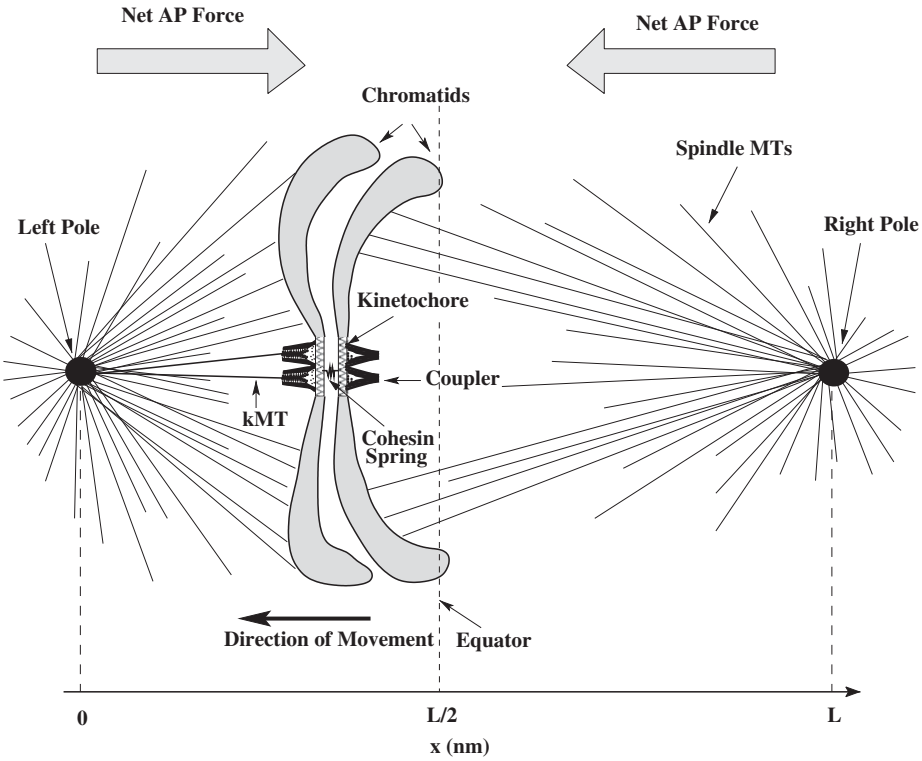

Fig. 1. Diagram of model components. For ease of illustration we have increased the relative scale of a chromosome in the cell. Polar-ejection forces (shown as large arrows) arise when the chromatids interact with microtubules that nucleate from two poles. These forces are directed away from each pole and thus create a centering effect. Each kinetochore in our model is equipped with up to 20 couplers; for simplicity we have shown only two per sister kinetochore. Sister chromatids are connected by a spring that maintains proper separation. The net polar ejection and spring forces exerted on a chromosome are read by each connected Kt motor that in turn responds with forces and velocities from its load–velocity curve.

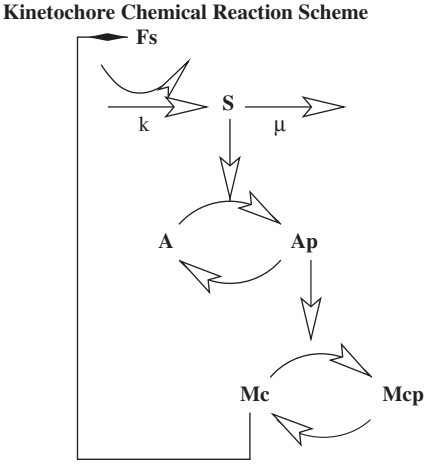

Fig. 2. Reaction diagram of the negative feedback loop between kinetochore loads (F_s) and chemical species reactions. Kinetochore loads increase sensor production (S), which in turn initiates a reversible two step phosphorylation cascade between the kinase (A) and kinesin (Mc).

In accordance with the above description, each kinetochore sensor species is activated at a load adaptive rate $k\sum_i F_{sj,i}(dx_j/dt, \beta_j(t))$, and decays with a constant rate μ,

$$\frac{dS_j}{dt} = k\sum_i F_{sj,i}\left(\frac{dx_j}{dt}, \beta_j(t)\right) - \mu S_j. \tag{4}$$

The two step phosphorylation cascade is modeled using Michaelis–Menten dynamics,

$$\frac{dAp_j}{dt} = \frac{k_A^+ S_j(A_{Tj} - Ap_j)}{K_A + A_{Tj} - Ap_j} - \frac{k_A^- Ap_j}{K_A + Ap_j}, \tag{5}$$

$$\frac{dMc_j}{dt} = \frac{-k_M^- Ap_j Mc_j}{K_M + Mc_j} + \frac{k_M^+(M_{Tj} - Mc_j)}{K_M + M_{Tj} - Mc_j}. \tag{6}$$

with $M_{Tj} = Mc_j + Mcp_j$, $A_{Tj} = A_j + Ap_j$, the total concentration of species Mc and A at kinetochore j. K_A, K_M are the Michaelis constants for the reactions. The rates k_A^-, k_M^+ characterize phosphatase kinetics whereas $k_A^+ S_j$, $k_M^- Ap_j$ are chosen so that maximum kinase velocities are reached when S and Ap are at their highest values. A similar cascade has been shown to cause limit cycle behavior for the cyclin-cdc2 kinase mitotic oscillator in Goldbeter (1991). The key characteristic of this cascade is that Ap and Mc show zero-order ultrasensitivity (i.e the reactions display sigmoidal switch-like signal-response curves) so that response increases continuously with signal strength and is fully reversible (Goldbeter and Koshland, 1981; Tyson et al., 2003).

Further, we assume that the microtubule depolymerization rate β_j at a given kinetochore is related to the amount of Mc available through the linear relationship

$$\beta_j(t) = \frac{\beta_{max} - \beta_{min}}{M_{Tj}} Mc_j + \beta_{min}. \tag{7}$$

Notice that the depolymerization rate β_j feeds back into the motor forces through the $F_{sj,i}(dx_j/dt, \beta_j)$ term of Eqs. (2) and (3) to report chemical species levels into the force balance calculation. Thus, we have feedback between chemical reactions and kinetochore forces.

Finally, we note here that in general our model is a system of eight nonlinear differential equations, but when one sister kinetochore is not attached (monooriented case) this system reduces to five equations since one set of chemical equations has trivial solutions.

2.1. Load velocity relationship for kinetochore diffusive motors

In this section we describe the key equations which were used to determine the load–velocity relationships for the biased diffusion motor (a more detailed description of this model is provided in another article).

Since the biological details of the Kt/MT interface are not completely understood, several theoretical models with various Kt attachment strategies have been proposed (Molodtsov et al., 2005; Efremov et al., 2007; McIntosh et al., 2008). One of the first theoretical treatments was by Hill (1985) who showed that biased thermal diffusion of Kt binders on a tethered MT lattice is sufficient to support continuous loads while keeping attachment to both growing and shortening MTs. Hill's molecular motor consisted of a rigid "sleeve" construct equipped with several weak MT binding sites. The sleeve structure is free to diffuse on the kMT lattice while the system seeks to minimize its energy by occupying as many sleeve binding sites as possible. Biased motion of the motor occurs because of depolymerization of the MT tip. For appropriate binding energies and sufficiently fast diffusion, the molecular motor is capable of bidirectional movement with velocities that depend on MT tip growth/shortening rates (Hill, 1985; Joglekar and Hunt, 2002). In his original treatment Hill required that the binding sites be arranged in a rigid narrow sleeve. This configuration does not allow for the flaring of MT ends that is seen during depolymerization. Nonetheless, the fundamental idea of biased diffusion can be incorporated into any arrangement of binding sites that are physically linked together (Powers et al., 2009).

In this paper we propose that coupling is accomplished by a modification of a diffusive Hill-type motor, the components of which are illustrated in Fig. 3A. The assumptions used to construct the motor model are as follows.

We assume that a motor is composed of a collection of fibers extending from the kinetochore with multiple binding attachments that can bind to sites on the MTs. The fibers are assumed to be sufficiently flexible so that they can attach to flaring microtubules. A coupler binder is also assumed to experience thermal motion (diffusion) on the lattice of an attached MT. Notice that since the binders are physically linked to each other on the fibers, it follows that the coupler experiences 1D diffusion on the polymer lattice.

Horizontal displacement for this motor is measured with respect to an internal motor frame of reference. The motor position variable, y, marks the distance between the polymer tip and the coupler end distal to the kinetochore plate. Thus, the position axis here starts at the coupler entry point ($y=0$ nm) and extends to the Kt plate ($y=50$ nm), as shown in Fig. 3A. The reason for this new frame of reference is that motor dynamics are directly dependent on the amount of overlap between the polymer and the coupler and not the specific chromosome position in the cell.

To characterize the binding interactions between the coupler and the polymer, we use an explicit energy landscape function, $\Psi(y)$. We suppose that each motor binder can weakly bind to a single monomer (i.e. there is a single binder binding site on each monomer). We position the binding sites so that when the polymer is fully inserted there are 65 occupied binding sites spread along 40 nm of the polymer. In agreement with Hill (1985) for an MT with 13 protofilaments with 8 nm long monomers, the binding sites are placed $\delta=8/13$ nm apart on the y-axis.

We now describe the structure of the potential well function (the exact expression of $\Psi(y)$ used here is given in the Appendix). The key assumption for potential well construction is that its shape should be such that additional binder attachments are energetically favored for the system. More specifically, for each new binding interaction established between the binders and the polymer, the system free energy is lowered by the amount " $-a$" , see Fig. 3A. On the other hand, in order for thermal motion to result in repositioning of the coupler relative to the polymer, existing bonds need to break. Bond breaking is not energetically favorable and thus imposes a potential barrier for each bond for movement, which we denote by "b" in the well, Fig. 3A. During insertion more bonds are established so that system free energy decreases in multiples of a, however, more bonds must also be broken so that the potential barrier increases in multiples of b. This produces a corrugated well $\Psi(y)$ with peaks and troughs varying linearly as y increases with the net effect of a drift term that biases thermal diffusion of the polymer inside the coupler.

But what happens if the polymer tip moves either by diffusion or polymerization past the last coupler binder? At this position there is no gain for the system to bias thermal motion in either direction since further insertion into the coupler does not lower the free energy-all possible binding sites are occupied. Nonetheless, if the coupler moves in this region it has to cross the potential barrier associated with breaking all bonds. Consequently, the potential well function $\Psi(y)$ loses its tilt and becomes periodic past the last binder position at $y=40$ nm as shown in Fig. 3A. The values for a, b are chosen small so that binding is weak and the barriers are low. This is done in order to allow for diffusion to easily relocate the MT tip to a lower energy state. We note here that motor behavior is not very sensitive to the specific values of the well parameters as long as the activation energies are kept much lower than the binding free energy.

Spindle forces acting on a chromosome as well as spring forces due to cohesins create mechanical stress on kinetochores producing load (F) on the motor. With our sign convention, $F>0$ pushes on a kinetochore to oppose poleward motion or equivalently pulls the polymer outside the coupler, whereas $F<0$ favors polymer insertion or poleward motion.

Finally, the tip of the inserted polymer is dynamic and can grow or shorten with prescribed rates that vary with the position of the tip relative to the kinetochore. A plot of the rates is shown in Fig. 3B. We assume that the depolymerase MCAK is enriched at the coupler end proximal to the kinetochore plate. Hence, we choose a depolymerization rate that depends on the position of the kMT tip relative to the motor (it varies from a basal value β_0 to a maximal value of β_j) and keep the polymerization rate constant (α_0), independent of tip position.

In the viscous-dominated limit, the motor system can be modeled with the forward Chapman–Kolmogorov equation,

$$\frac{\partial p(y,t)}{\partial t}=\frac{\partial}{\partial y}\left\{\left[\frac{\Psi'(y)}{v}+\frac{F}{v}\right]p(y,t)\right\}+\alpha(y-\delta)p(y-\delta,t)+\beta(y+\delta)p(y+\delta,t)-(\alpha(y)+\beta(y))p(y,t)+D\frac{\partial^2}{\partial y^2}p(y,t), \quad (8)$$

where $p(y,t)$ is the probability density function for y, the relative MT tip position. D is the kinetochore diffusion coefficient, v is the effective kinetochore viscosity and $\alpha(y)$, $\beta(y)$ are position dependent polymerization and depolymerization rates for the kMT tip. Notice that Eq. (8) includes jump terms coming from the addition or removal of monomers of size δ in addition to diffusion and drift. This equation is similar to a model of a polymerization ratchet proposed by Peskin et al. (1993) with the difference that here we have an explicit binding energy potential $\Psi(y)$ and the tip depolymerization rate is position dependent.

For a given depolymerization rate β_j and reasonable loads, a motor sustains attachment to an MT. Since the polymer tip is constantly growing/shortening, attachment produces movement of the motor with respect to the x-axis. Notice, however, that so far, all the coupler equations have been written in terms of the

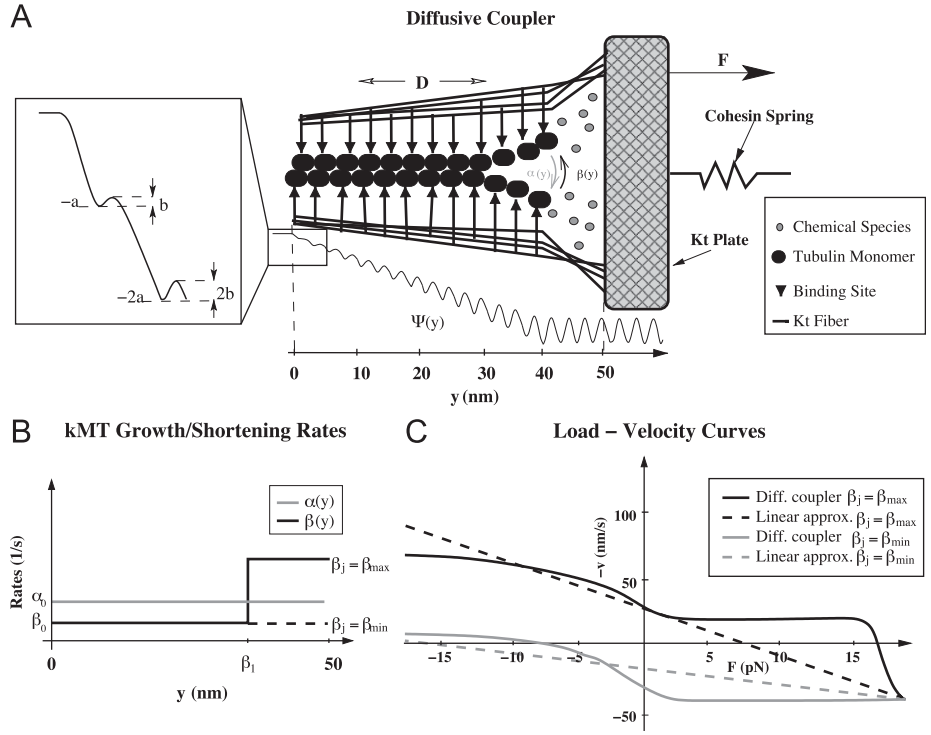

Fig. 3. (A) Diffusive coupler diagram. Several weak kMT lattice binding sites diffuse on an inserted microtubule with a dynamic tip. The energy of binding is represented by a potential well function $\Psi(y)$ which creates a bias for increased overlap between the kinetochore filaments and the polymer. Motor loads (F) coming from polar ejection forces and the spring oppose the potential well bias for insertion. (B) The polymerization/depolymerization rates for the tip of an inserted MT are position dependent functions. The polymerization rate is constant whereas the depolymerization rate is a step function that varies from β_0 to β_j. β_j depends on the concentration of active MCAK at the kinetochore. (C) Load–velocity curves for the diffusive couplers and their respective linear approximation. For the diffusive motors load velocity curves for are mostly flat. The linear load–velocity curves have the same quantitative behavior as the nonlinear load–velocity curves when the rate β_j varies. The rate β_j for the linear curves was chosen to give a good fit to the nonlinear case; all other rate parameters are the same. In this plot $-v>0$ denotes poleward or depolymerization-driven motion, whereas $-v<0$ denotes antipoleward or polymerization-driven motion.

relative position variable, y. Yet, in order to incorporate this motor into the cell we have to measure its movement with respect to the cell's frame of reference, x. The average velocity of an attached motor with respect to the x-axis is calculated as the sum of the average velocity of movement of the MT tip given by the balance between α and β, plus the average velocity of movement of the Kt relative to the kMT tip,

$$v(F,\beta_j)=\frac{d}{dt}\langle x_K\rangle=\frac{d}{dt}\langle x_p\rangle+\frac{d}{dt}\langle y\rangle,$$
$$=\delta\int(\alpha(y)-\beta(y))p(y,t)\,dy+\int y p_t(y,t)\,dy, \tag{9}$$

where x_K, x_P are the Kt plate and MT polymer tip positions, respectively, in the x frame of reference.

For our chosen parameters, the attractive forces coming from the potential well create a metastable state in which the position of the tip relative to the coupler is fixed. This implies that at steady state the coupler moves (relative to the x-axis) with an average velocity that equals the balance of kMT tip rates. If we let $p_s(y)$ be the corresponding steady state probability density (which is obtained by solving Eq. (8) with left hand side set to zero with appropriate boundary conditions), the velocity expression reduces to

$$v(F,\beta_j)=\delta\int(\alpha(y)-\beta(y))p_s(y)\,dy. \tag{10}$$

We use Eq. (10) to determine load–velocity curves for the motors. Two representative load–velocity curves are shown in Fig. 3C (note that we plot $-v(F,\beta_j(t))$ in the y-axis of these graphs).

The key feature of the load–velocity curves is the wide range of loads for which the velocity is nearly constant. This arises due to the dependence of the steady state distributions on the force term, F. In Fig. 4 we show the numerical solutions shown as normalized histograms representing the steady state distributions calculated for various amounts of load on the motor. For ease of visualization the microscopic corrugated well effects on the histograms have been filtered out to highlight the macroscopic behavior of the system when the value F is varied. Note from Eq. (8) that the load term F can act directly to either enhance or diminish the well force effect $\Psi'(y)$ depending on its sign. Consequently, the steady state distribution for the position of the polymer tip, $p_s(y)$ experiences shifts on the y-axis as a result of changes in the load on the motor. However, notice from Figs. 3C and 4 that the velocity does not change as long as the values of the tip rates in this shifted position remain unchanged. This is due to the fact that the velocity of this motor is determined by the balance of MT growth/shortening rates at the equilibrium tip position. Effectively, the coupler does not change its velocity unless the loads are such that the tip is in the regions where the balance of rates changes. Thus, as in Hill (1985), our model provides a mechanism by which the coupler responds to a wide range of loads with constant velocities.

In Fig. 4 observe that the polymerization rate has to drop to zero when the distance between the polymer tip and the Kt plate is less than δ, since monomers cannot be added unless there is enough space to do so. This imposes a transition to higher motor depolymerization velocities in the load–velocity plot as the polymer is pushed with more force ($F<0$) against the plate. This is because it is harder for the MT to add monomers against a large pushing load—however, depolymerization still proceeds

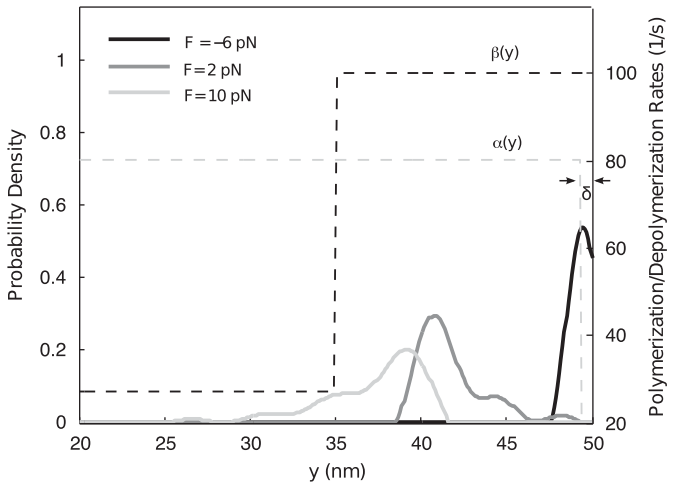

Fig. 4. Steady state distributions for various system loads, F, compared with kMT tip growth/shortening rates. For each force value, Eq. (8) is solved numerically and the histograms (smoothed to eliminate microscale details) are plotted (solid lines). For these simulations $\beta_j = 100\,s^{-1}$, and the remaining parameters are the same as in Table 1. MT tip polymerization/depolymerization rate functions are shown with dashed lines.

Table 1
Parameter values.

Parameter	Description	Value
L	Cell diameter	40 μm (Skibbens et al., 1993)
v	Effective viscous drag coefficient	6 pNs/μm (Joglekar and Hunt, 2002)
k	Sensor response rate to load	.02 nM/pN s (estimated)
μ	Sensor decay rate	.05 s^{-1} (estimated)
$k_M^- = k_A^+$	Maximum kinase reaction velocity	.1 s^{-1} (Tyson et al., 2003)
$k_M^+ = k_A^-$	Maximum phosphatase reaction velocity	.2 nM/s (Tyson et al., 2003)
$K_A = K_M$	Michaelis rate constants	.01 nM (Tyson et al., 2003; Goldbeter, 1991)
L_k	Cohesin spring relaxed length	1000 nm (Waters et al., 1996)
k_f	Cohesin spring coefficient	.1 pN/nm (Joglekar and Hunt, 2002)
α_0	Rate of tubulin subunit addition	80 s^{-1} (Joglekar and Hunt, 2002)
β_0	Basal rate of tubulin subunit removal	27 s^{-1} (Joglekar and Hunt, 2002)
β_{max}	Max. rate of removal of tubulin	130 s^{-1} (estimated)
β_{min}	Min. rate of removal of tubulin	27 s^{-1} (estimated)
a	Free energy of binding	2.6 k_BT (Hill, 1985)
b	Unit activation barrier	.01 k_BT (Powers et al., 2009)
D	Coupler diffusion coefficient	690 nm/s^2 (Hill, 1985)
F_{max}	Linear load–velocity curve constant force factor	18 pN (estimated)

unaffected (see Fig. 3C). Therefore, in this force regime the motor effectively responds like a polymerization ratchet in agreement with the results of Peskin et al. (1993). On the other hand, when the pulling forces ($F > 0$) are significant, parts of the steady state distributions localize in regions where the polymerization rate is greater than the depolymerization rate. This produces a decline in depolymerization velocities in the load–velocity curves when $\beta_j > \alpha_0$ since in Eq. (10) there is a contribution in the velocity integral for regions where $\alpha(y) > \beta(y)$. Of course, if the pulling loads increase too much the motor breaks down with the polymer pulled out of the motor. Thus the pulling force range in the velocity calculation must be restricted accordingly.

Finally, we note that the expression in Eq. (10) cannot be evaluated to find explicit relationships between motor velocity v, the rate β_j and load F. Furthermore, for Eqs. (2) and (3), we need the load as a function of velocity and β_j, and these equations are implicit rather than explicit equations for chromosome velocity. We can greatly simplify the analysis of our model by replacing the diffusive motor load–velocity curves coming from solutions of (8)–(10) with explicit relationships that retain key characteristics of the motor. Thus, in addition to solving the full model (numerically) we also explore the behavior of the model when the motor load–velocity relationships are given by the linear equation,

$$F_{sj,i}(v_j, \beta_j) = \frac{2F_{max}}{\delta(\beta_0 - \beta_j - \alpha_0)}\left(v_j - \frac{\delta(\beta_j + \beta_0 - \alpha_0)}{2}\right). \tag{11}$$

A comparison between the load velocity curves of the biased diffusion couplers and the linear Eq. (11) is shown in Fig. 3C. Notice that the linear curves show the same qualitative behavior as the numerically determined diffusive coupler curves for β_j between β_{min} and β_{max}.

3. Results

We numerically solved the model equations to track chromosome positions and chemical species levels as functions of time.

For the simulations, local kinetochore species concentrations were scaled by S_θ and normalized $S_\theta = M_{Tj} = A_{Tj} = 1$. Kinetic and binding parameter values were either taken directly from the literature or estimated from experimental data (see Appendix). A complete list of model parameters is shown in Table 1. For the simulations of the system with linear load velocity curves the variables were rescaled and the results are presented in terms of $\chi_j = x_j/L$, $s_j = S_j/S_{max}$, $a_j = Ap_j/A_T$, $m_j = Mc_j/M_T$, $\tau = t/T$.

3.1. Feedback with diffusive couplers predicts oscillations for monooriented chromosomes

We first calculated solutions for kinetochores equipped with up to 20 attachments at each kinetochore as suggested by data from Newt Lung cells (Skibbens et al., 1993), then we repeated our calculations with the linear load–velocity curves and analyzed model behavior.

The plots in Fig. 5 display model solutions for the position of each sister chromatid, sensor, load per motor, and kinase/kinesin levels as a function of time. For these solutions only the left kinetochore is allowed to attach motors to kMTs, i.e., the chromosome is monooriented.

In Fig. 5A we show the simulated motion of a chromosome with the left chromatid positioned initially at $x = 15\,\mu m$. The left kinetochore is allowed to establish 1–2 new attachments every 100 s. Independent of the initial chromosome position, the model predicts an initial approach to the pole and then movement with very regular poleward and antipoleward excursions with speeds $\approx 1.8\,\mu m/min$ in each direction (amplitude $\approx 2\,\mu m$, period ≈ 3 min) matching experimental observations in Newt Lung cells (Skibbens et al., 1993).

The characteristic constant velocity poleward and antipoleward excursions seen in our simulations are a consequence of the flatness of the load velocity curves on which kinetochore diffusive couplers operate. A load increase results in a shift in the maximal probability for the position of the tip inside the coupler. However, if kMT dynamic rates in this shifted position are unchanged chromosome velocity remains constant. On the other hand, if the

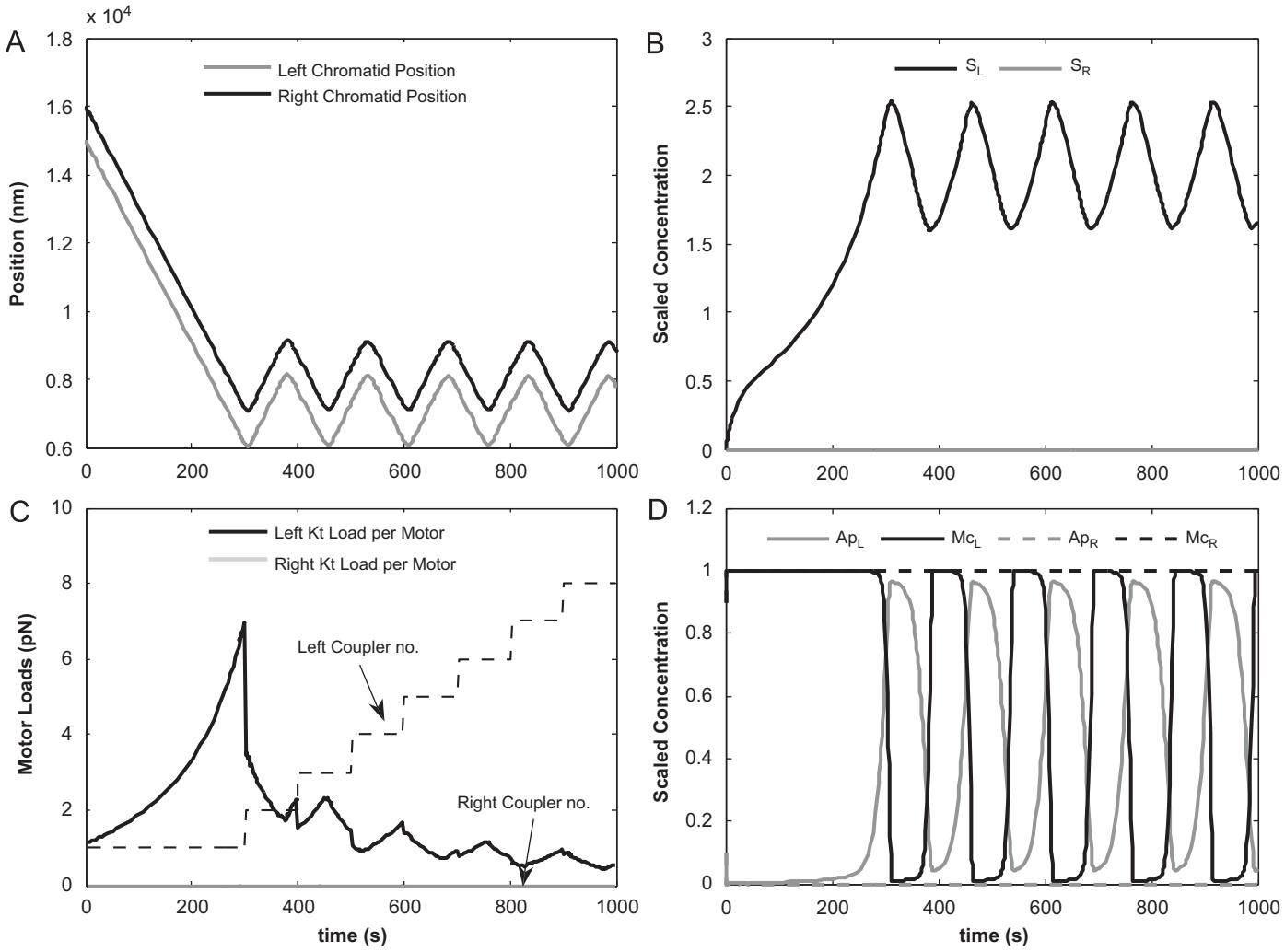

Fig. 5. Monooriented chromosome directional instability. (A) Chromatid positions are controlled by respective feedback loops acting on the diffusive couplers. The left pole is located at $x=0$. The initial conditions for sister chromatids are: $x_L=15\,\mu m$; $x_R=16\,\mu m$; $S_L=S_R=0$; $Ap_L=Ap_R=0.1$; $Mc_L=Mc_R=0.9$. (B and D) Chemical species levels during chromosome oscillations. (C) Motor numbers and loads per motor at each Kt.

depolymerization rate (β_j) is altered, coupler load–velocity curves shift so chromosome velocities change. In our case since Mc controls the depolymerization rate β_j and it quickly switches between either zero or fully active levels, the couplers essentially operate on two load–velocity curves: one where the depolymerization rate is at its highest (depolymerizing movement) and the other where the depolymerization rate is at its basal level (polymerizing movement), see Fig. 3C.

In Fig. 5 C we plot the load felt by each attached left Kt motor as a function of time. The addition of new attachments redistributes loads by lowering the burden on each coupler. However, this does not affect motion as long as load variations remain within the flat region of the load–velocity curves. This implies that all motors respond with the same velocities despite individual load variations. Furthermore, since new attachments do not affect total load (and thus the local chemical reactions), the model predicts regular monooriented oscillations that are insensitive to the number of attachments at a kinetochore.

As can be seen from the sensor species concentrations plotted in Fig. 5B, "directional instability" for monooriented chromosomes is a direct byproduct of sensor species oscillations. Sensor species oscillations occur due to the change in the balance of forces as the chromosome changes position. The oscillations in sensor levels turn on or off the bicyclic cascade switch, as shown in Fig. 5D. If a kinetochore moves to a location where the load it feels increases, then the sensor reaches its threshold value S_θ faster. Once above threshold, S levels force A to fully activate by mediating its phosphorylation into Ap which subsequently turns off the depolymerase Mc. The time necessary for Ap to build up and Mc to shut down is the time allocated for direction switch in our model. Consequently, the kinetic parameters for kinases and phosphatases are chosen to match the sharp chromosome directional changes (≈ 6 s Skibbens et al., 1993). When Mc is inactive the diffusive coupler is in polymerizing state driving antipoleward motion, which causes the couplers to feel less load, S decays below S_θ and the phosphorylation cascade switch is reversed so that monooriented directional instability is established.

It should be noted that the reaction cascade we propose here exhibits threshold dependent switching behavior. Oscillations are not sustained if Ap and Mc activation curves lack the necessary zero order ultrasensitivity, which is controlled by K_m values as predicted in Goldbeter and Koshland (1981). In Fig. S1 we plot chromatid positions for different values of phosphorylation

reaction kinetic parameters. The model predicts monooriented chromosome oscillations for a wide range of parameter values provided there are sufficiently sharp thresholds in the activation of the kinase and kinesin species. It should be noted that it is likely that more steps are involved in the cascade than our minimal representation. Increasing the number of cascade steps could produce sharper thresholds in activation since sensitivity is amplified in subsequent cycles (Goldbeter and Koshland, 1981) resulting in a possible increase of oscillation robustness.

For the system with linear load velocity curves we obtain similar monooriented oscillations. In Fig. S2 we plot the system solutions for the position and kinetochore chemical levels of a monooriented chromosome with linear load–velocity curves. The system produces monooriented oscillations independent of the initial chromosome position, with some slight differences in movement arising from the shape of the load–velocity curves. As expected, velocities are not constant, this is especially noticeable in the initial left pole approach while motor loads increase. The variation of velocity becomes apparent when the sensor production rate is slightly decreased, as shown in Fig. S3. Also, in contrast to the diffusive coupler motors, for the system with linear load–velocity curves the addition of new connections affects the shape of monooriented oscillations since motor load variation imposes changes in velocity. Clearly, the diffusive coupler model is a much more adequate model for the coupling mechanism, although the linear load–velocity approximation retains qualitative model behavior for the monooriented case.

In conclusion, our model suggests that monooriented oscillations could be the result of a local kinetochore load sensor driving fast switch-like phosphorylation cascades.

3.2. The feedback mechanism predicts congression for bioriented chromosomes

In Fig. 6 we show the model solutions for which the right kinetochore is allowed to accumulate attachments so that the chromosome becomes bioriented.

In Fig. 6A is shown the simulated motion of a chromosome which is initially monooriented (7 left couplers attached) and becomes bioriented at $t = 900\,\mathrm{s}$ when one right kinetochore coupler is engaged. Observe that the chromosome immediately changes direction and follows the right (leading) kinetochore with persistent motion away from the pole covering distances of $\approx 10\,\mu\mathrm{m}$ in a few minutes, in accordance with experimental observations in Skibbens et al. (1993).

A comparison between sister kinetochore positions and chemical levels (Fig. 6B, D) shows that the movement of sister chromatids follows the evolution of their respective chemical reactions. At the onset of biorientation, coupler motors at each sister kinetochore feel forces in opposing directions. The right kinetochore motor experiences a strong ejection gradient which pushes the kMT tips inside the coupler so that the right coupler responds with right pole directed (poleward) motion. The left couplers, on the other hand, feel large opposing AP loads which result in antipoleward velocities slightly smaller in magnitude than right coupler velocities. This difference produces immediate stretch on the center spring which increases the spring forces on both motors. However, only the left motors feel a significant pulling load and sensor increase since the AP gradient absorbs the spring force effects on the right coupler, as seen in Fig. 6C. After the initial spring force spike, if the AP force gradient remains strong then right kinetochore motors continue to respond with poleward velocities, whereas the left kinetochore motors keep high sensor levels due to high loads. Consequently, both motors move with almost the same magnitude velocities toward the equator according to load velocity relationships. It is important to highlight here that congression in our model is insensitive to the amounts of trailing kinetochore sensor at the time of biorientation (figures not shown).

In fact, the distance traveled by a congressing bioriented chromosome depends on the strength of the ejection forces. In Fig. S4 we show model solutions for high and low levels of polar ejection force gradients. We observe that for very weak AP forces a bioriented chromosome experiences oscillations close to the poles, essentially failing to congress. This is because the trailing kinetochore does not feel enough load to keep S from going below threshold and it attempts poleward trips at the onset of congression. However, once ejection forces build up, AP movement persists allowing for fast equator approach, as seen in experiments. This implies that the AP gradient strength directs congression by controlling the length of antipoleward trips and not velocity differences, in good agreement with observations in Skibbens et al. (1993).

A comparison of attached motor numbers on each sister chromatid from Fig. 6C shows that congression is achieved despite the trailing kinetochore having far more motors attached than the leading one. Our simulations show that for the same values of the AP gradient, increasing the number of trailing kinetochore attachments does not significantly affect congression. More attachments on the trailing kinetochore produce more initial resistance to congression followed by sharp spring responses. However, if the AP forces can quickly counteract spring forces and keep sensor levels sufficiently high the trailing kinetochore moves antipoleward and congression progresses independent of the number of attachments. Therefore, the model suggests that the AP gradient is necessary and sufficient to assign a leading kinetochore independent of attachment numbers.

Interestingly, chemical species reactions show that sister kinetochores have very different levels of phosphorylated Mc during congression as seen in Fig. 6D. Our simulations show a situation where the leading kinetochore always has all Mc active (unphosphorylated) whereas the trailing one has little active Mc (all phosphorylated) as it approaches the equator. This model behavior is particularly interesting since experiments have shown that Aurora B inexplicably phosphorylates MCAK asymmetrically across centromeres showing an accumulation of active MCAK at the leading kinetochore during congression (Andrews et al., 2004; Kline-Smith et al., 2004). It has been proposed that congression could be mediated by asymmetries in active MCAK levels (Andrews et al., 2004; Gorbsky, 2004). Nonetheless, there is to date no clear mechanistic explanation as to why such differences in MCAK activity levels across kinetochores may occur. Our model predicts that asymmetries could be the result of inequalities in the dynamics of kinetochore chemical reactions caused by AP induced load differences across sister kinetochores.

Substitution of the load–velocity curves with linear functions does not change system behavior significantly during congression. In Fig. S5 we show the simulated chromatid motion and respective chemical species levels of a chromosome that becomes bioriented at $\tau = 60$. Even though a chromosome congresses to the equator, linear load–velocity curves can cause early onset of right kinetochore congression opposing trips (seen in Fig. S5A). This arises due to the fact that in the linear load–velocity curve case, direction reversal is achieved for different loads as compared to the nonlinear case (i.e different x-intercept for each curve in Fig. 3 C). Thus, when AP forces weaken closer to the equator, smaller amounts of resistive spring forces cause the right motors to reverse into polymerizing motion than in the nonlinear case. In summary, the shape of the load–velocity curves affects the speed of congression through its triggering of resistive poleward trips during equatorial approach.

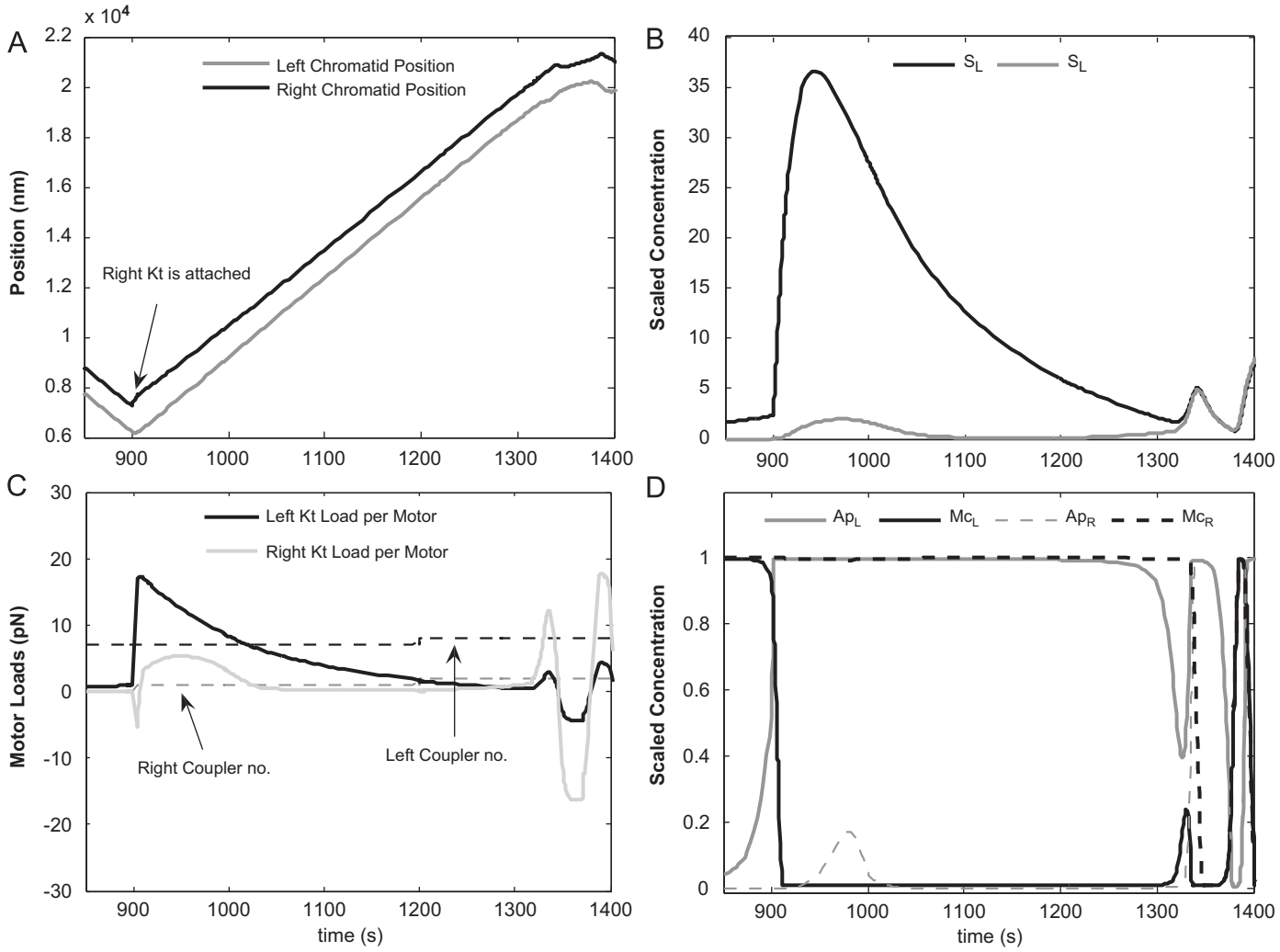

Fig. 6. Bioriented congression. (A) The position of a chromosome which becomes bioriented at $t=900$ s. For the polar ejection forces, f_{ap} is increased to allow for congression rates seen in Skibbens et al. (1993). Despite unequal attachment numbers, a leading Kt is established and congression is achieved. (B and D) Chemical species levels during chromosome oscillations. (C) Motor numbers and loads per motor at each Kt.

3.3. *Post congression, bioriented chromosomes oscillate with smaller amplitudes, higher frequencies and can pause*

In Fig. 7A, 7C, 7E, 7G are shown model solutions for times after the initial congression has occurred.

Once a bioriented chromosome moves close to the equator the AP force gradient weakens and center spring forces become significant. Because of the load feedback response, as a chromosome gets closer to the equator, the motors prolong the congression-opposing states during which they test the AP gradient. Bioriented oscillations take place only if the AP gradient is weak enough for the motors to directly oppose each other so that both kinetochore sensors increase above threshold (intra-Kt tension takes over spatial cues). Sensors fully synchronize at the equator where there is no AP gradient bias, as seen in Fig. 7C. Bioriented oscillations tend to be in-phase when there is a significant difference in the numbers of couplers engaged at each kinetochore, shown in Fig. 7A. These in-phase movements are due to the difference in loads as seen in Fig. 7G and subsequently the coupler velocity response of each sister chromatid. If the number of attached motors at each kinetochore is the same they all pick equal speeds for equal loads. So, as the differences in velocities decrease, kinetochores are forced into out-of-phase trips driven by sensor synchronization at the equator followed by periods of no movement where both kinetochores are polymerizing slowly against the center spring (neutral). In our simulations, the maximal amplitude of oscillations for bioriented in-phase and out-of-phase oscillations is $\approx 1\,\mu$m and the period is $\approx 1-1.5$ min. The amplitudes of these oscillations are smaller than the ones reported in Skibbens et al. (1993), this is due to our choice of kMT polymerization and depolymerization rates. With higher kMT tip rates the amplitudes increase to closer match experimental observations.

In Fig. 8 system solutions are displayed for a bioriented chromosome at the equator with linear load–velocity curve motors. The feedback mechanism in this case produces nearly identical bioriented oscillations, shown in Fig. 8A, as simulations in Fig. 7A for the fully nonlinear coupler.

In conclusion our model predicts oscillations around the cell equator for bioriented chromosomes. The phase relationship between sister kinetochores seems to depend on the number of attachments established on each kinetochore. Unequal numbers of attachments produce in-phase oscillations similar to the ones seen in experiments. For equal numbers of attachments phases of no motion are seen, similar to those seen in experiments during bioriented oscillations but not during monooriented oscillations in Newt lung cells (Skibbens

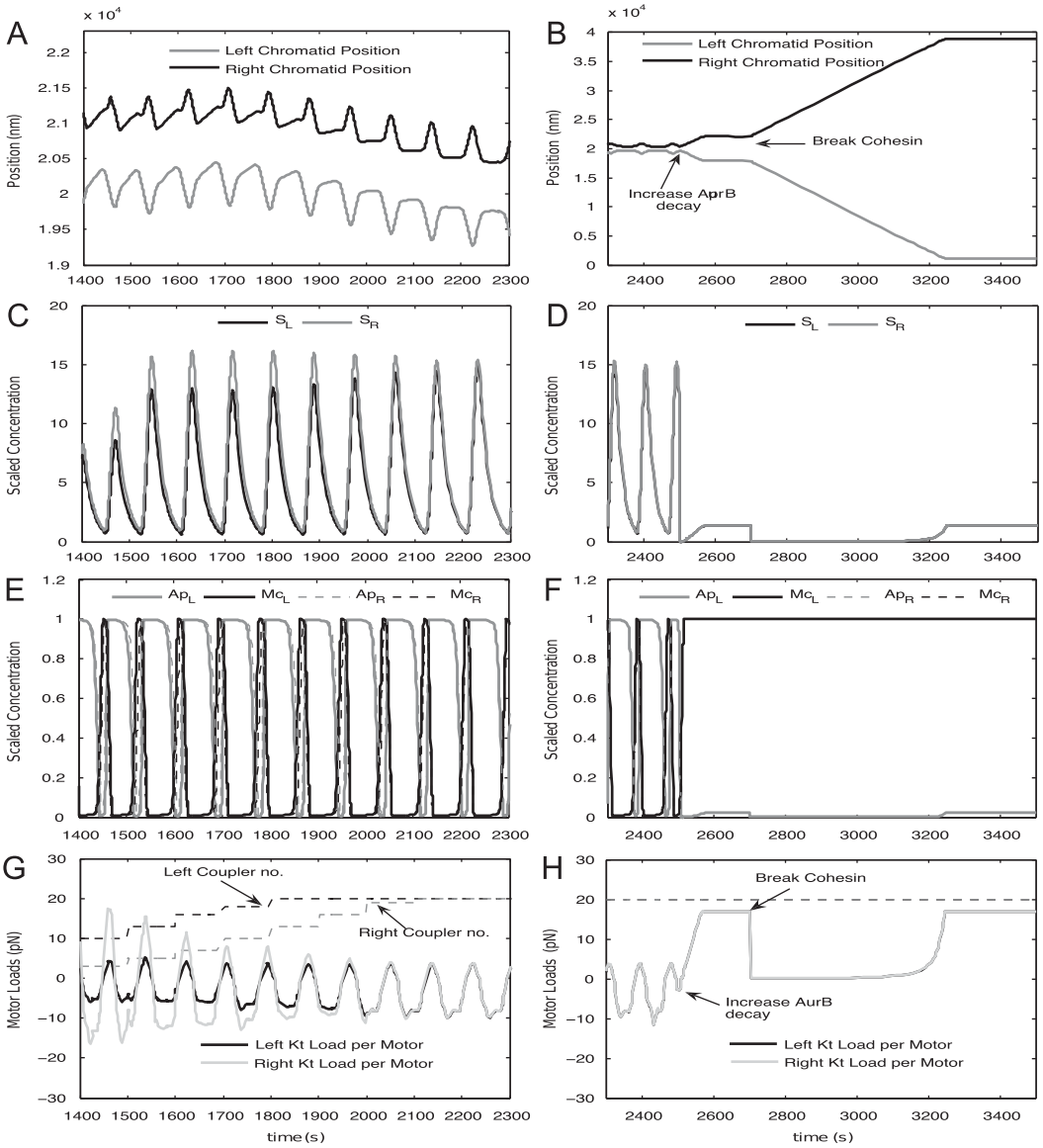

Fig. 7. Bioriented chromosome oscillations and anaphase transition. (A and B) After congression bioriented chromosome oscillations are sustained at the equator when the sensor is properly localized. (C and D) Sensor species levels during oscillations and after sensor and spring removal. (E and F) Chemical species levels during bioriented chromosome oscillations at the equator. (G and H) Loads per motor and attached motor numbers for each kinetochore. In panel B, D, F, H reaction parameters change as follows: (1) $t=2500$ s sensor decay rate increases from $\mu=.05\,s^{-1}$ to $5\,s^{-1}$ and oscillations cease with the chromosome stretched and precisely centered. (2) $t=2700$ s the cohesin spring is removed with $k_f=0$ allowing for chromosome segregation.

et al., 1993). Unequal numbers of attachments on sister kinetochores produce oscillations centered slightly away from the equator. However, when a chromosome steers too far from the equator AP centering cues become stronger than intra-centromeric tension which decreases sensor synchrony and causes quick trip interruptions that bias position toward the equator. This implies that attachment number variation can slightly offset centering until the chemical reactions can build a response to the AP gradient that points the chromosome back to the equator. Nonetheless, once the attachment numbers become nearly equal on each side, the chromosome always returns to oscillating around the equator independent of the strength of the polar ejection gradient.

3.4. Metaphase/anaphase transition

So far we have discussed model results with the assumption that the chemical species included in the feedback remain localized at kinetochores. However, if the sensor species is interpreted as part of the chromosome passenger complex (CPC) then we should take into account that the position of this complex varies depending on the particular stage of cell division (Ruchaud et al., 2007). Since we integrate the action of this chemical species in movement control, we can use our model to test whether variation in species localization agrees with movement phenotypes observed in mitotic cells.

Once all chromosomes are properly aligned at the equator, AurB-INCENP relocates from centromeres to the spindle midzone microtubules due to Cyclin B degradation upon anaphase-start signal release (Murata-Hori et al., 2002). We can investigate the effects of this relocation in our model by allowing for quick sensor removal, i.e. by increasing the decay rate μ. In Fig. 7B, D, F, H we show model solutions extended after equatorial alignment as a function of time while model parameters are varied sequentially. In Fig. 7B we show a plot of the position of each chromatid where at time $t=2500$ s the sensor decay rate is significantly increased.

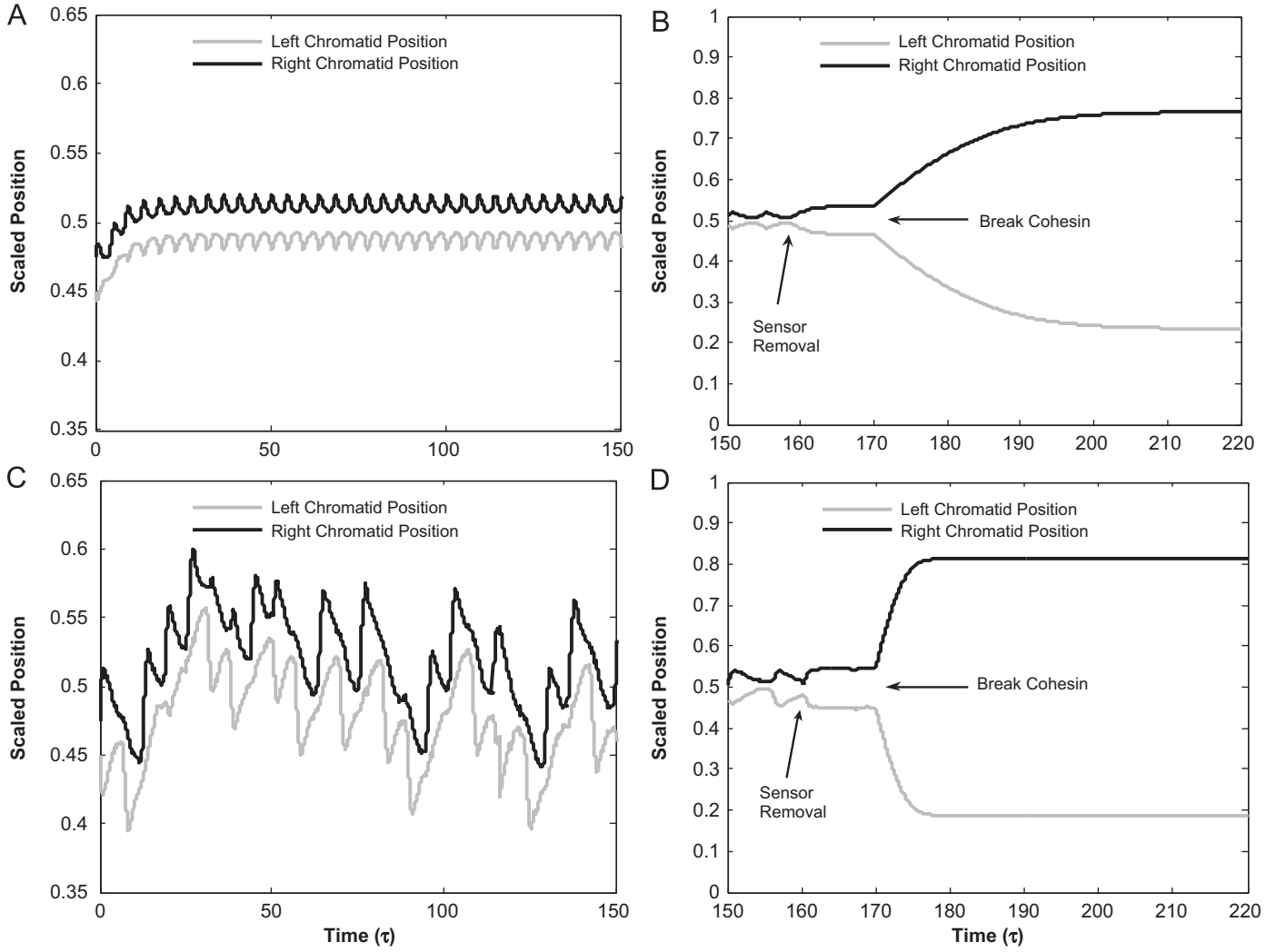

Fig. 8. Bioriented chromosome oscillations and cellular noise effects for the system with linear load–velocity equations. (A and C) Bioriented chromosome oscillations are sustained at the equator when the sensor is properly localized. Each kinetochore has 20 attachments with initial conditions $\chi_L = .45$; $\chi_R = .475$; $s_L = s_R = 0$; $A_L = A_R = 0.1$; $m_L = m_R = 0.9$. In panel C noise is introduced in the system and the depolymerization rate β_{max} is increased to allow for higher amplitude oscillations. (B and D) System response to feedback breakdown and spring removal. Reaction parameters change as follows: (1) $\tau = 160$, the nondimensional parameter $k_1 = k_4 k F_{max}/\mu^2 = 14.4$ is reduced to $k_1 = 0.000144$ and oscillations cease with the chromosome stretched and precisely centered even when the system experiences random velocity variations. (2) $\tau = 170$ the cohesin spring is removed by setting the parameter $\gamma_4 = k_f/v\mu = 0$ allowing for chromosome segregation.

Accordingly, oscillations stop and the chromosome is precisely positioned at the equator with high centromeric stretch. This behavior is explained by Fig. 7D, F that show sensor levels below threshold and low kinase activity. The kinetochores thus pull against the polar ejection gradient until their couplers reach their stall loads. Thus, fast removal of sensor predicts a stretched conformation as a precursor to anaphase pole migration. However, as can be seen in Fig. 9 where we have plotted solutions of the system with moderate μ rate, if removal is not very fast the system experiences oscillations with high centromeric stretching. In cells depleted of centromeric MCAK both stretch and oscillations were observed at the onset of anaphase (Kline-Smith et al., 2004). We predict that both these experimental observations could be the result of different levels of feedback disassembly at kinetochores.

The final step for transition from metaphase to anaphase requires the protease separase to cleave a cohesin subunit allowing for sister chromatid separation (Uhlmann, 2001). There is evidence that transition into anaphase poleward movement might not only entail the breaking of the linking cohesins but also proper modulation of kinetochore chemical reactions. The reintroduction of Cyclin B in cohesin cleaved chromosomes can cause AurB-INCENP to not relocalize producing interesting chromosome movement phenotypes such as oscillations around a pseudometaphase plate (Parry et al., 2003). Further, experiments that vary Cyclin B doses in cells show that a separated chromatid can either oscillate or experience stand-still behavior at different locations in the cell depending on polar-ejection strength (Wolf et al., 2006). Both experiments seem to indicate that kinetochore reactions (more specifically AurB removal) control anaphase movement phenotypes. We can easily test whether our model captures these experimental observations.

In Fig. 7B we show the movement of a bioriented chromosome after cohesin removal ($k_f = 0$) at time $t = 2700$ s. Notice that poleward movement is sustained upon separation and reaction disassembly. However, if the sensor is not quickly removed oscillations occur due to the feedback response to load. In Fig. 9 we have plotted the movement of a chromosome which undergoes separation when the removal of the sensor is slow; close to the poles oscillations persist. Our model produces both stand still and oscillatory movement at the equator for separated chromatids if the polar ejection forces are kept strong (figures not

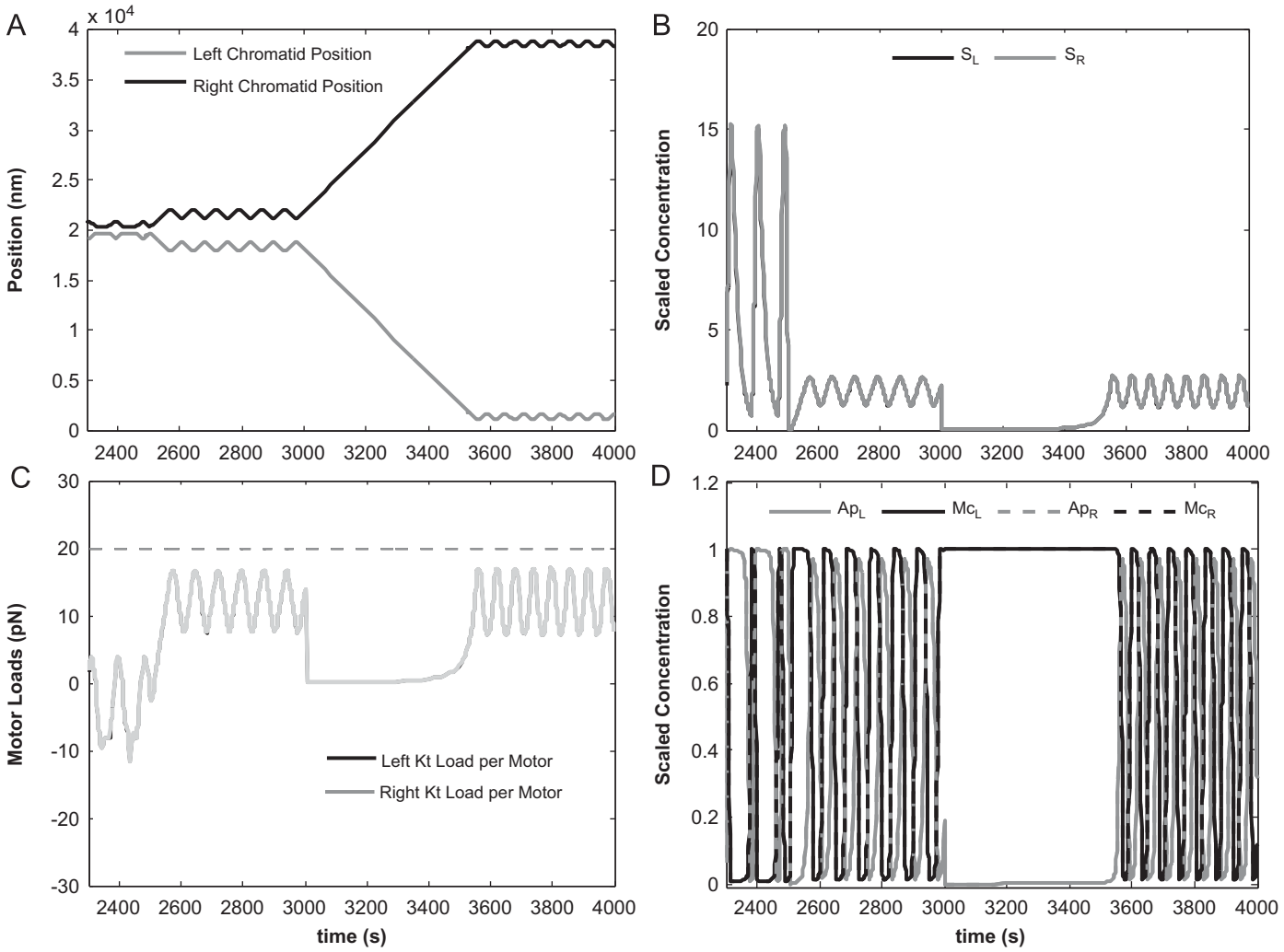

Fig. 9. Bioriented chromosome oscillations at the equator for slow sensor relocation. (A) Chromosome position. (B and D) Chemical species levels at each kinetochore. (C) Load per motor and motor attachment numbers at each kinetochore. The reaction parameters change as follows: (1) at $t=2500$ s sensor decay rate increases from $\mu=.05\,s^{-1}$ to $2.5\,s^{-1}$ and oscillations persist with the chromosome stretched and precisely centered. (2) at $t=3000$ s the cohesin spring is removed with $k_f=0$ allowing for chromosome segregation.

shown). If the feedback is partially operating after separation, oscillations persist close to the pole for weak polar ejection forces, or at a pseudometaphase plate if the force gradient is strong. If the removal of the sensor is complete then the chromatid loses oscillatory behavior and moves to a new equilibrium position where the motors stall, which can be either close to the pole or the equator depending upon the strength of the polar forces. Therefore, our results indicate that anaphase transition for chromosomes is not purely a force balance problem. Indeed, our model predicts that persistent anaphase poleward movement has a strong chemical component, which when interpreted as feedback disassembly, agrees well with experimental observations.

The relocation of the sensor produces the same stretching effects for the system with linear load–velocity equations as for the nonlinear load–velocity curves and finally the removal of the spring causes persistent poleward trips. In panel B of Fig. 8, model parameters are changed so that at $\tau=160$ there is faster sensor removal and at $\tau=170$ the cohesin spring is removed. Just as in the nonlinear load–velocity curve motor case, if the sensor is not removed quickly enough the chromatids oscillate close to their respective poles after segregating (figure not shown).

In conclusion, the shape of the load–velocity curve does not significantly change the behavior of the negative feedback system. As long as the couplers can move with velocities that depend upon kMT tip rates, the negative biochemical feedback mechanism produces monooriented oscillations, congression, bioriented oscillations and proper segregation.

3.5. Feedback response to noise

Cells are noisy environments so a more realistic model of chromosome movement has to take into account some stochastic effects. Since the linearized system retained all the features of the implicit nonlinear model, we can easily explore the effects of noise on the system by perturbing the velocity equations (Eq. (10)) with Gaussian distributed noise terms $\xi_i(t)$ (see Appendix). In Fig. 8C, which shows the position of the chromatids of a bioriented chromosome, we see that the addition of noise causes the appearance of more in-phase oscillations at the equator. This is due to the random variation of sensor values which can delay the phosphorylation switch response forcing kinetochores into in-phase movements. The noise induced

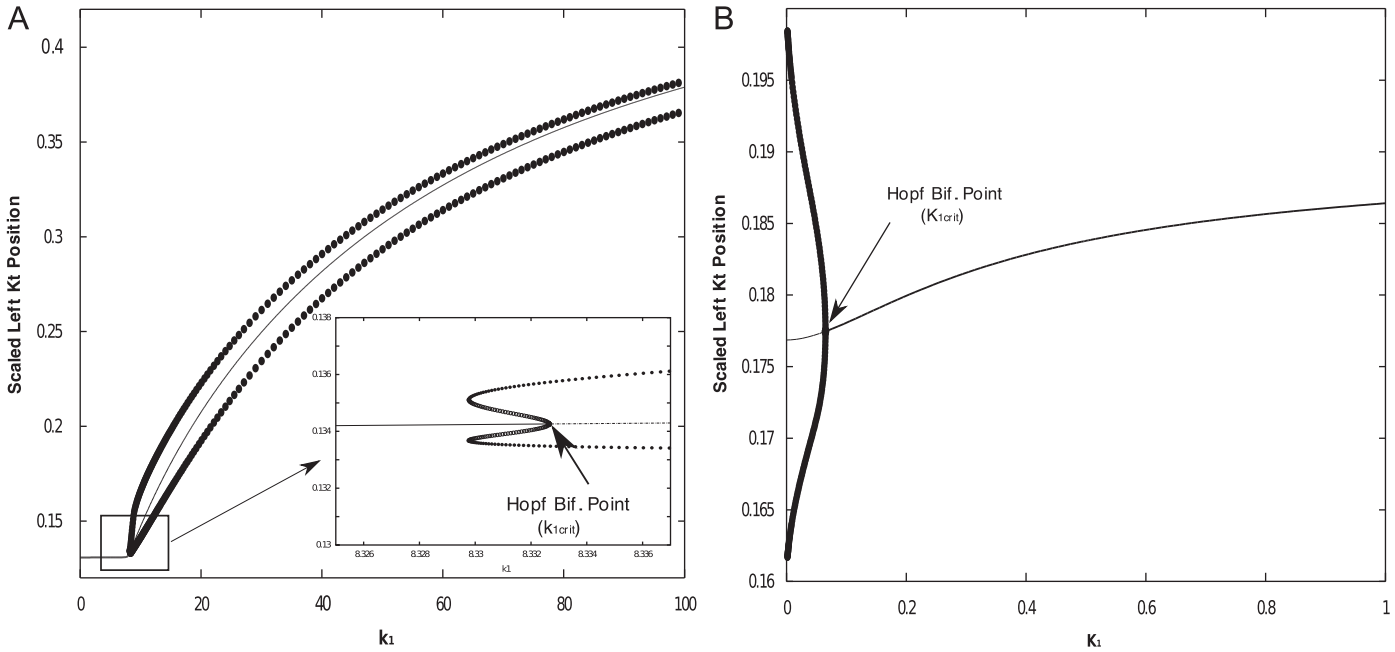

Fig. 10. Bifurcation diagrams for a monooriented chromosome with linear load–velocity curves. Solid line depicts stable steady states, dashed line represents unstable steady states. Filled circles represent stable periodic solutions whereas open circles represent unstable periodic solutions. (A) Steady state response of the left chromatid position, χ_L as a function of the parameter k_1. Inset. For a small interval of k_1 close to the Hopf bifurcation point the system experiences hysteresis. (B) Steady state response of χ_L as a function of the parameter K_1.

in-phase oscillations are in very good agreement with observations in Newt Lung cells (Skibbens et al., 1993).

It is important to note that noise does not affect the precise centering of a chromosome at the equator after sensor relocation. This can be seen from the solutions plotted in Fig. 8D where sequential parameter variation produces solutions which are very similar to those of the system without noise in Fig. 8B. This implies that our biochemical feedback is robust to noise and an appropriate control mechanism in noisy cellular environments.

3.6. Feedback is robust to parameter variation

The response of the negative feedback mechanism depends on the value of a few key kinetic parameters. These parameter values, however, have not been experimentally measured so it is important to explore system robustness to parameter variations. Since the linearized system retains qualitative behavior of the full model we can use it to explore the robustness of the feedback and its general dynamic properties.

In this section we investigate the behavior of our system under variations of the dimensionless parameters: $k_1 = k_A^+ kF_{max}/\mu^2$, $K_1 = K_A/A_T = K_M/M_T$. These two parameters were chosen since they directly control monooriented and bioriented oscillations as follows: (1) the parameter k_1 encodes the strength of position cues into the feedback so its variation should affect system behavior and (2) the value of K_1 affects the delay in the feedback coming from kinase/kinesin switch and consequently controls the onset of oscillations.

In Fig. 10 we have plotted the bifurcation diagrams of a monooriented chromosome (only one attachment at the left Kt) with respect to the parameters k_1 and K_1. Oscillations are sensitive to kinase/kinesin switch sharpness since a periodic branch appears for a small range of K_1, as seen in Fig. 10B. However, once the value of K_1 is less than $K_{1\text{crit}}$ the system produces stable periodic solutions for a wide range of $k_1 > k_{1\text{crit}}$, Fig. 10A. Clearly, as k_1 increases the system becomes more sensitive to spatial cues and a monooriented chromosome will tend to oscillate closer to the equator. If the system is made extremely sensitive then any amount of AP gradient will cause even a monooriented chromosome to oscillate at the equator (the periodic branch asymptotes to $\chi = 0.5$ in Fig. 10A). Thus, the model predicts that if too much sensor (AurB) is recruited at an attached kinetochore a monooriented chromosome can be forced to the equator immediately without the need for biorientation. Also observe in Fig. 10 (inset) that around the Hopf bifurcation at $k_{1\text{crit}}$ the system experiences a brief hysteresis. This arises due to the nonlinearities in the feedback mechanism.

In Fig. 11 we show the bifurcation diagram of a bioriented chromosome which has one motor attached at each kinetochore with respect to the variables k_1, K_1. Sister chromatid coupling with linear springs introduces more complex dynamics in the system. The variation of feedback sensitivity in Fig. 11C generates two Hopf bifurcation points and a period doubling bifurcation for small values of k_1. The doubling of the period for $k_{1h1} < k_1 < k_{1p}$ indicates that if the system is made fairly insensitive to spatial cues it can take longer for a chromatid to complete an oscillation until it stops oscillating if k_1 is too small. The stable steady state branch for $k_1 < k_{1h1}$ shows that each kinetochore settles in a stretched position as the feedback is being disassembled. The unstable periodic branch that appears for this system ($k_1 > k_{1h2}$, Fig. 11A, C) shows interesting dynamic properties, however, such behavior is due to the nonlinearity of the system and it is of no biological consequence due to lack of stability. Variation of K_1 in Fig. 11B shows two periodic branches in the bioriented case, however, since the second branch is not stable it does not affect chromosome oscillation dynamics at the equator. Note that the oscillatory domain with respect to the parameter K_1 has expanded compared to the monooriented system.

We conclude by noting that bifurcation analysis indicates that monooriented and bioriented oscillations are robust to parameter variations once the kinase/kinesin switch is sufficiently sharp.

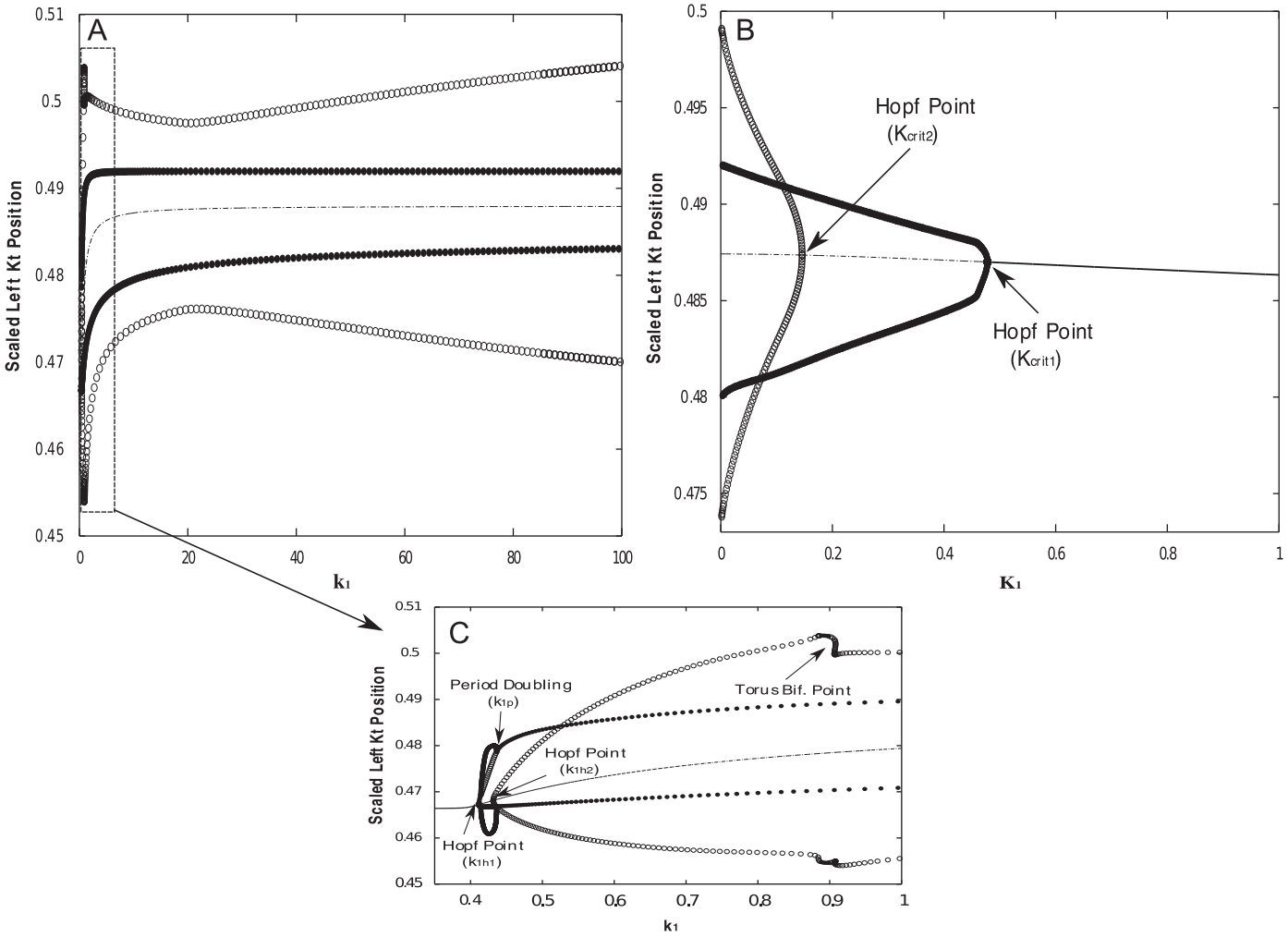

Fig. 11. Bifurcation diagrams for the bioriented case with linear load–velocity curves. Solid line depicts stable steady states, dashed line represents unstable steady states. Filled circles represent stable periodic solutions whereas open circles represent unstable periodic solutions. To simplify the diagram we have only shown the position of the left chromatid, χ_L since the right kinetochore shows identical dynamics with positions shifted to the right due to spring separation. (A) Steady state response of the left kinetochore position, χ_L as a function of the parameter k_1. (B) Steady state response of χ_L as a function of the parameter K_1.

4. Discussion

During mitosis both mechanical forces and chemical signals are implicated in the accurate division of chromosomes. Mechanical forces directing congression arise from polar ejection forces which increase loads on sister chromatids when poles are approached. Several kinases localized at kinetochores are thought to read load information and change their activation states via phosphorylation reactions. Finally, substrates of kinetochore kinases can alter attached kMT tip dynamics which in turn modulates Kt velocities.

In this paper we propose a feedback control mechanism which integrates mechanical and chemical signals at kinetochores to recreate chromosomal movement. Even though there could be several Kt kinases that phosphorylate/dephosphorylate in a force dependent manner we model motility by reducing all possible interactions into three simple reactions: a mechanical load reader species that activates/deactivates in response to loads, a kinase that experiences (auto)phosphorylation in response to sensor activation, and a kMT tip rate altering species that is regulated by the kinase. Chemical species levels are introduced into a diffusive coupler model which yields a molecular scale treatment of kMT tip dynamics coupling to chromosomal velocities. The well observed CPC-Aurora B-MCAK system could be the most direct representation of a possible complex network of load-sensing and kMT tip rate modulation species. With parameters estimated from mitosis experiments, our simple network predicts many experimentally observed features of vertebrate chromosomal movement for both monooriented and bioriented states. The system shows robustness to parameter variation as well as cellular noise effects.

Previous theoretical models have successfully captured different aspects of chromosome motility in various organisms. The models of Joglekar and Hunt (2002) for Newt lung cells and Civelekoglu-Scholey et al. (2006) for *Drosophila* embryos are based on a force balance mechanism for chromosome motility. In our study, we sought to combine these mechanical force effects with local kinetochore reactions. Indeed, a force balance mechanism might be sufficient to generate oscillatory behavior, however, a kinetochore biochemical feedback mechanism might be necessary to assure robust monooriented oscillations, equatorial alignment and proper transition between different mitotic stages.

The limit cycle behavior produced by our model is different from the response produced by a biochemical feedback control mechanism recently proposed in Liu et al. (2008). We suspect that these differences are more likely to occur due to the introduction of load dependence on velocities rather than biochemical

feedback topology differences. Consequently, we predict that the introduction of kinetochore motors in a biochemical feedback model can significantly affect chromosome motility.

If the biochemical feedback control we propose here indeed controls mitotic motion then the question about its functional significance naturally arises. Many proteins that localize at kinetochores are part of the spindle assembly checkpoint (SAC), a complex quality control network which blocks anaphase until all chromosomes are properly attached (Ruchaud et al., 2007; Musacchio and Salmon, 2007). There is evidence that Aurora B either directly or through the CPC affects mitotic spindle checkpoint proteins which build a tension sensitive SAC signal (Morrow et al., 2005; Ruchaud et al., 2007). In our model, at the onset of biorientation each kinetochore has different levels of the kinase A, but when the chromosome is fully centered, bioriented sister kinetochores sensors are fully synchronized. It could be that the presence of a feedback mechanism with kinases like AurB allows for a chemical signal build up to indicate that a specific chromosome is ready for separation. How such a signal can be transduced and how tension modulates it is not well known (Ruchaud et al., 2007; Musacchio and Salmon, 2007). It would be interesting to investigate possible integration of chromosomal movement with SAC dynamics.

Acknowledgment

This Research was supported in part by the National Science Foundation Grant DMS-0718036.

Appendix A

A.1. Simplifying assumptions

We model the motion of only one chromosome. In Newt Lung cells with several chromosomes there could be interactions between motile chromosomes. We do not take any such interactions into account.

We assume that the biochemical reaction species are localized at the kinetochores i.e. do not diffuse in the cytoplasm.

We assume that each kMT is attached to a pole which has a fixed position (i.e. constant pole to pole distance). Also we ignore any flux effects at MT minus ends.

Each coupler can only support a certain amount of load before the attachment is lost. We can show that the coupler can support up to 18 pN of load for the chosen parameters before the maximal probability distributions settle outside the coupler region. Even though the amount of force a single coupler can support is small compared to spindle forces, since Newt Lung cell kinetochores can bind up to 20 microtubules (Skibbens et al., 1993), a fully attached kinetochore supports up to 360 pN of load. This load range is a limitation of the coupler model that arises from the weak interactions with binding sites.

Polar ejection forces are assumed to be density dependent and thus modeled with a smooth distribution as in Joglekar and Hunt (2002). It is likely that this force distribution varies more with position and time, which in our context would produce less regular oscillations. Chromosome arms contain chromokinesin motors which are thought to contribute in the generation of polar ejection forces. We do not directly model fluctuations in chromokinesin motor activity.

A.2. Potential well for the motor

Note that in agreement with Hill (1985) and Joglekar and Hunt (2002) we position the binding sites so that a fully attached coupler binds 65 sites along 40 nm of the polymer lattice with each site separated by $\delta = 8$ nm per monomer/13 protofilaments. The equation for the well is given by,

$$\Psi(y) = \begin{cases} 0, & 0 \le x < \frac{\delta}{2}, \\ (n-1)\left(-\frac{3a}{2} + \frac{b}{2} - \frac{b+a}{2}\cos\left(\frac{2\pi x}{\delta}\right)\right), & \frac{(2n-1)\delta}{2} \le x < n\delta, \\ n\left(-a + \frac{b}{2} - \frac{b}{2}\cos\left(\frac{2\pi x}{\delta}\right)\right), & n\delta \le x < \frac{(2n+1)\delta}{2}, \end{cases}$$

A.3. Cohesin spring stiffness

For our cohesin springs we used the spring coefficient estimated by Joglekar and Hunt (2002) of .1 pN/nm and a relaxed intra-kinetochore distance of 1 μm as measured in Waters et al. (1996). The magnitude of the spring coefficient dictates sister kinetochore coupling during bioriented movement. We tested several values and observed that if the spring coefficient is lowered to 0.001 pN/nm coupling is almost completely lost with bioriented oscillations looking like monooriented oscillations around the equator. Higher spring coefficients (up to .2 pN/nm) on the other hand, enhance sister chromatid coupling but also lower oscillation amplitudes since loads are greatly increased when a kinetochore tries to initiate movement away from the equator. Intermediate values allow for both coupling and reasonable amplitudes. Furthermore, we have imposed repulsion for springs compressing more than L_k, which corresponds to a physical barrier that does not allow chromosome arms to get closer than what has been observed experimentally.

A.4. Chemical reaction parameter estimation

We estimated the parameters for growth and decay of S so that the amplitude and frequency of monooriented chromosome oscillations (which are the most regular ones) matched data from Newt lung cells in Skibbens et al. (1993). For the kinetic parameters of the bicyclic phosphorylation cascade we use the values of K_A, K_M, k_A^+, k_A^-, k_M^-, k_M^+ estimated in Tyson et al. (2003), similar to the cascade parameters for cyclin and cdc2 kinase in Goldbeter (1991). These parameters give the needed time delays for chromosomal directional switches.

A.5. Congression and AP force gradient

For the simulation of the monooriented chromosome the AP force density factor is decreased to allow the chromosome to move close enough to the pole to which it is attached. Lower gradients can be justified since it takes time for the astral microtubules to grow enough to exert forces on the arms so that AP forces gain strength as mitosis progresses. Thus, we envision this gradient to gain strength over time. For congression the factor was increased to allow timely equator approach. After congression is achieved the AP gradient is increased to reach the measured value of ≈ 100 pN at 2 μm from the equator (Brouhard and Hunt, 2005).

A.6. System with noise

To study the effects of noise we include the stochastic forcing term $\xi(t)$ with $\langle \xi_i \rangle = 0$, $\langle \xi_i(t_1), \xi_i(t_2) \rangle = \sigma_i^2 \delta(t_1 - t_2)$ which perturbs the velocity of each kinetochore. The equations of motion (1) are modified to be of the form

$$v\frac{dx_i}{dt} = \sum F + \xi(t). \tag{12}$$

In the simulations the noise level is adjusted to be such that $\sigma_i/V_{max} = .06$, where V_{max} is the effective maximal velocity the system reaches when there is no noise.

Appendix B. Supplementary data

Supplementary data associated with this article can be found in the online version at doi:10.1016/j.jtbi.2009.12.023.

References

Andrews, P.D., Ovechkina, Y., Morrice, N., Wagenbach, M., Duncan, K., et al., 2004. Aurora B Regulates MCAK at the mitotic centromere. Dev. Cell 6, 253–268.

Bolton, M.A., Lan, W., Powers, S.E., McCleland, M.L., Kuang, J., et al., 2002. Aurora B kinase exists in a complex with survivin and INCENP and its kinase activity is stimulated by survivin binding and phosphorylation. Mol. Biol. Cell 12, 3064–3077.

Brouhard, G.J., Hunt, A.J., 2005. Microtubule movements on the arms of mitotic chromosomes: polar ejection forces quantified in vitro. Proc. Natl. Acad. Sci. USA 102, 13903–13908.

Cheeseman, I.M., Desai, A., 2008. Molecular architecture of the kinetochore–microtubule interface. Nat. Rev. Mol. Cell Biol. 9, 33–46.

Civelekoglu-Scholey, G., Sharp, D.J., Mogilner, A., Scholey, J.M., 2006. Model of chromosome motility in drosophila embryos: adaptation of a general mechanism for rapid mitosis. Biophys. J. 90, 3966–3982.

Efremov, A.K., Grishchuk, E.L., McIntosh, R.I., Ataullakhonov, F.I., 2007. In search of an optimal ring to couple microtubule depolymerization to processive chromosome motions. Proc. Natl. Acad. Sci. USA 104, 19017–19022.

Ems-McClung, S.C., Hertzer, K.M., Zhang, X., Miller, M.W., Walczak, C., 2007. The interplay of the N- and C-terminal domains of MCAK control microtubule depolymerization activity and spindle assembly. Mol. Biol. Cell 18, 282–294.

Gardner, M.K., Pearson, G., Sprague, B., Zarzar, T., Bloom, K., et al., 2005. Tension-dependent regulation of microtubule dynamics at kinetochores can explain metaphase congression in yeast. Mol. Biol. Cell 16, 3764–3775.

Goldbeter, A., 1991. A minimal cascade model for the mitotic oscillator involving cyclin and cdc2 kinase. Proc. Natl. Acad. Sci. USA 88, 9107–9111.

Goldbeter, A., Koshland, D., 1981. An amplified sensitivity arising from covalent modification in biological systems. Proc. Natl. Acad. Sci. USA 78, 6840–6844.

Grishchuk, E.L., McIntosh, J.R., 2006. Microtubule depolymerization can drive poleward chromosome motion in fission yeast. EMBO J. 25, 4888–4896.

Gorbsky, G.J., 2004. Mitosis: MCAK under the aura of Aurora B. Curr. Biol. 14, 346–348.

Hill, T.L., 1985. Theoretical problems related to the attachment of microtubules to kinetochores. Proc. Natl. Acad. Sci. USA 82, 4404–4408.

Joglekar, A.P., Hunt, A.J., 2002. Simple mechanistic model for directional instability during mitotic chromosome movement. Biophys. J. 83, 42–58.

Kapoor, T.M., Lampson, M.A., Hegert, P., Cameron, L., Cimini, D., et al., 2006. Chromosomes can congress to the metaphase plate before biorientation. Science 311, 388–391.

Kline-Smith, S.L., Khodjakov, A., Hergert, P., Walczak, C., 2004. Depletion of centromeric MCAK leads to chromosome congression and segregation defects doe to improper kinetochore attachments. Mol. Biol. Cell 15, 1146–1159.

Lampson, M.A., Renduchitala, K., Khodjakov, A., Kapoor, T.M., 2004. Correcting improper chromosome-spindle attachments during cell division. Nat. Cell Biol. 6, 232–237.

Liu, J., Desai, A., Onuchic, J.N., Hwa, T., 2008. An integrated mechanobiochemical feedback mechanism describes chromosome motility from prometaphase to anaphase in mitosis. Proc. Natl. Acad. Sci. USA 105, 13752–13757.

McIntosh, J.R., Grishchuk, E.L., Morphew, M.K., Efremov, A.K., Chudenkov, V.A., et al., 2008. Fibrils connect microtubule tips with kinetochores: a mechanism to couple tubulin dynamics to chromosome motion. Cell 135, 322–333.

Mitchison, T.J., Salmon, E.D., 1992. Poleward kinetochore fiber movement occurs during both metaphase and anaphase-a in Newt lung cell mitosis. J. Cell Biol. 119, 569–582.

Molodtsov, M.I., Grischchuk, E.L., Efremov, A.K., McIntosh, J.R., Ataullakhonov, F.I., 2005. Force production by depolymerizing microtubules: a theoretical study. Proc. Natl. Acad. Sci. USA 102, 4353–4358.

Morrow, C.J., Tighe, A., Johnson, V.L., Scott, M.I.F., Ditchfield, C., et al., 2005. Bub1 and Aurora B cooperate to maintain BubR1-mediated inhibition of APC/C/Cdc20. J. Cell Sci. 118, 3639–3652.

Murata-Hori, M., Tatsuka, M., Li-Wang, Y., 2002. Probing the dynamics and functions of Aurora B kinase in living cells during mitosis and cytokinesis. Mol. Biol. Cell 13, 1099–1108.

Murata-Hori, M., Wang, Y., 2002. The kinase activity of Aurora B is required for kinetochore–microtubule interactions during mitosis. Curr. Biol. 12, 894–899.

Musacchio, A., Salmon, E.D., 2007. The spindle-assembly checkpoint in space and time. Nat. Rev. Mol. Cell Biol. 8, 379–393.

Parry, D.H., Hickson, G.R.X., O'Farrell, P.H., 2003. Cyclin B destruction triggers changes in kinetochore behavior essential for successful anaphase. Curr. Biol. 13, 647–653.

Peskin, C.S., Odell, G.M., Osters, G.F., 1993. Cellular motions and thermal fluctuations: the Brownian ratchet. Biophys. J. 65, 316–324.

Powers, A.F., Franck, A.D., Gestaut, D.R., Cooper, J., Gracyzk, B., et al., 2009. The Ndc80 kinetochore complex forms load-bearing attachments to dynamic microtubule tips via biased diffusion. Cell 136, 865–875.

Rieder, C.L., Davison, E.A., Jensen, L.C., Cassimeris, L., Salmon, E.D., 1986. Oscillatory movements of monooriented chromosomes and their position relative to the spindle pole result from ejection properties of the aster and half spindle. J. Cell Biol. 103, 581–591.

Rieder, C.L., Salmon, E.D., 1994. Motile kinetochores and polar ejection forces dictate chromosome position on the vertebrate mitotic spindle. J. Cell Biol. 124, 223–233.

Ruchaud, S., Carmena, M., Earnshaw, W.C., 2007. Chromosomal passengers: conducting cell division. Nat. Rev. Mol. Cell Biol. 8, 798–812.

Sandall, S., Severin, F., McLeod, I.X., Yates, J.R., Oegama, K., et al., 2006. A Bir1-Sli15 complex connects centromeres to microtubules and is required to sense kinetochore tension. Cell 127, 1179–1191.

Skibbens, R.V., Petrie-Skeen, V., Salmon, E.D., 1993. Directional instability of kinetochore motility during chromosome congression and segregation in mitotic newt lung cells: a push pull mechanism. J. Cell Biol. 122, 859–875.

Tanaka, K., Kitamura, E., Kitamura, Y., Tanaka, T.U., 2007. Molecular mechanisms of microtubule-dependent kinetochore transport toward spindle poles. J. Cell Biol. 178, 269–281.

Tyson, J.J., Chen, K.C., Novak, B., 2003. Sniffers, buzzers, toggles and blinkers: dynamics of regulatory and signaling pathways in the cell. Curr. Opin. Cell Biol. 15, 221–231.

Uhlmann, F., 2001. Secured cutting: controlling separase at the metaphase to anaphase transition. EMBO Rep. 2, 487–492.

Waters, J.C., Skibbens, R.V., Salmon, E.D., 1996. Oscillating mitotic Newt lung cell kinetochores are, on average, under tension and rarely push. J. Cell Sci. 109, 2823–2831.

Wolf, F., Wandke, C., Isenberg, N., Geley, S., 2006. Dose-dependent effects of stable Cyclin B1 on progression through mitosis in human cells. EMBO J. 25, 2802–2813.

Wordeman, L., Wagenbach, M., von Dassow, G., 2007. MCAK facilitates chromosome movement by promoting kinetochore microtubule turnover. J. Cell Biol. 179, 869–879.